Acta Crystallographica Section B
**Structural Science**
ISSN 0108-7681

# On the crystal structure of $Cr_2N$ precipitates in high-nitrogen austenitic stainless steel. III. Neutron diffraction study on the ordered $Cr_2N$ superstructure

**Tae-Ho Lee,[a]* Sung-Joon Kim,[a] Eunjoo Shin[b] and Setsuo Takaki[c]**

[a]ECO-Materials Research Center, Korea Institute of Machinery and Materials, 66 Sangnam, Changwon 641-010, Republic of Korea, [b]HANARO, Korea Atomic Energy Research Institute, PO Box 105, Yuseong, Daejeon 305-600, Republic of Korea, and [c]Department of Materials Science and Engineering, Kyushu University, 744 Motooka, Nishi-ku, Fukuoka 812-8581, Japan

Correspondence e-mail: lth@kmail.kimm.re.kr

Received 14 April 2006
Accepted 25 August 2006

Part I: Lee, Oh, Han, Lee, Kim & Takaki (2005). *Acta Cryst.* B**61**, 137–144. Part II: Lee, Kim & Takaki (2006). *Acta Cryst.* B**62**, 190–196.

The ordered structure of $Cr_2N$ precipitates in high-nitrogen austenitic steel was investigated utilizing high-resolution neutron powder diffractometry (HRPD). On the basis of the Rietveld refinement of neutron diffraction patterns, the ordered $Cr_2N$ superstructure was confirmed to be trigonal (space group $P\bar{3}1m$), with lattice parameters $a$ = 4.800 (4) and $c$ = 4.472 (5) Å, as suggested in previous transmission electron microscopy studies [Lee, Oh, Han, Lee, Kim & Takaki (2005). *Acta Cryst.* B**61**, 137–144; Lee, Kim & Takaki (2006). *Acta Cryst.* B**62**, 190–196]. The occupancies of the N atoms in four crystallographic sites [1($a$), 1($b$), 2($d$) and 2($c$) Wyckoff sites] were determined to be 1.00 (5), 0.0, 0.74 (9) and 0.12 (3), respectively, reflecting a partial disordering of N atoms along the $c$ axis. The position of the metal atom was specified to be $x$ = 0.346 (8) and $z$ = 0.244 (6), corresponding to a deviation from the ideal position ($x$ = 0.333 and $z$ = 0.250). This deviation caused the $(\frac{1}{3}\frac{1}{3}0)$-type superlattice reflection to appear. A comparison between the ideal and measured crystal structures of $Cr_2N$ was performed using a computer simulation of selected-area diffraction patterns.

## 1. Introduction

Precipitation reactions of second phases have been regarded as one of the most important features in austenitic stainless steels, because their mechanical and corrosion properties are profoundly dependent on the formation of precipitates (Lee *et al.*, 2000; Peckner & Bernstein, 1987; Weiss & Stickler, 1972). In the case of austenitic high-nitrogen steels, it is reported that the main precipitate is $M_2X$-type nitride ($M$ = Cr, Mo, Fe and Mn; $X$ = N and C) (simply designated as $Cr_2N$), and the precipitation of $Cr_2N$ occurs in various forms of intergranular (along grain boundaries), cellular and intragranular (within grains) precipitation depending on aging conditions (Kikuchi *et al.*, 1991; Simmons, 1996; Lee *et al.*, 2004*a*,*b*). Although extensive literature is available concerned with the effect of nitrogen on precipitation (Kikuchi *et al.*, 1991; Lee *et al.*, 2000) together with its detrimental effects on steel properties (Gavriljuk & Berns, 1999; Simmons, 1996; Vanderschaeve *et al.*, 1995), no systematic studies on the crystal structure of $Cr_2N$ have been carried out.

It is known that the crystal structures of transition-metal carbides and nitrides are based on face-centered cubic (f.c.c.) or hexagonal close-packed (h.c.p.) sublattices of metal atoms with interstitial atoms occupying some of the octahedral interstices (Ducastelle, 1991; Khachaturyan, 1978, 1983; Nagakura & Oketani, 1968). The $\varepsilon$-type ordering has been reported to be a typical ordered structure in hexagonal interstitial compounds, and the stacking sequence of the (0001) plane along the $c$ axis can be expressed as

$A_M\alpha_I B_M\beta_I\ldots$, (where $\alpha_I$ and $\beta_I$ are the two types of basal layers occupied by interstitial atoms; $A_M$ and $B_M$ are the h.c.p. sublattice of metal atoms; Epicier *et al.*, 1988; Hendricks & Kosting, 1930; Jack, 1952; Leineweber & Jacobs, 2000). Hendricks & Kosting (1930) first found a $(\frac{1}{3}\frac{1}{3}1)$-type superlattice reflection in the Fe–N system and suggested an increased $3^{1/2} \times 3^{1/2} \times 1$-type superstructure based on the geometrical arrangements of Fe octahedra. Jack (1952) confirmed the $\varepsilon$-type ordering for a wide range of Fe–N compositions and proposed a model for the continuous structural transition from $\varepsilon$-$Fe_3N$ to $\varepsilon$-$Fe_2N$. Subsequently, numerous studies on these $\varepsilon$-type ordered structures have been carried out in other alloy systems, such as $Mo_2C$, $W_2C$ (Epicier *et al.*, 1988), $Ta_2C$ (Lönnberg *et al.*, 1986), $V_2C$, $Nb_2C$ (Hiraga & Hirabayashi, 1980) and $ZrO_x$ ($0.3 < x < 0.5$) (Hirabayashi *et al.*, 1974), and five ordered superstructures [$P\bar{3}m1$, $P\bar{3}1m$ (trigonal), *Pnnm*, *Pbcn* and *Pnma* (orthorhombic)] have been proposed depending on the configurations of the interstitial atoms (Epicier *et al.*, 1988; Hiraga & Hirabayashi, 1980). Furthermore, the crystallographic features as well as order–disorder transitions depend on the specific configurations of interstitial atoms within the aforementioned ordered structures (Ducastelle, 1991; Epicier *et al.*, 1988; Khachaturyan, 1983; Nagakura & Oketani, 1968).

For the Cr–N system, Lee *et al.* (2005) found three sets of superlattice reflections in TEM–SADP (transmission electron microscopy–selected area diffraction pattern) analyses and proposed a modified occupation probability function for describing the nitrogen distribution using the static concentration waves method suggested by Landau & Lifshitz (1980) and Khachaturyan (1978, 1983). In addition, the irradiation-induced disordering of $Cr_2N$ during electron irradiation was found, for the first time, and a model for the order–disorder transition was suggested, based on the disappearing sequence of superlattice reflections (Lee *et al.*, 2006). However, from the crystallographic point of view, complementary studies need to be carried out in that (i) the accurate atomic coordinates of the substitutional elements were not specified and (ii) the occupancies of the N atoms in four crystallographic sites were not determined. To fill these deficiencies, in the present study, a neutron diffraction study on the ordered $Cr_2N$ superstructure was carried out, and a comparison between the ideal and measured $Cr_2N$ superstructures was made utilizing computer simulations of SAD patterns.

## 2. Experimental

The investigated material was a commercial high-nitrogen austenitic P900NMo alloy (manufactured by VSG, Germany) with the following composition in wt%: 17.94 Cr; 18.60 Mn; 2.09 Mo; 0.89 N; 0.04 C; balance Fe. Specimens were sealed in a quartz tube under vacuum and solution-treated at 1423 K for 30 min in the austenite ($\gamma$) single-phase region (Lee *et al.*, 2004*b*); this process was followed by water quenching. Specimens were isothermally aged at 1173 K for $10^5$ s in an argon atmosphere and quenched in water. This aging condition was chosen because the microstructure consisted mainly of only a $\gamma$ matrix and the $Cr_2N$ precipitate (Lee *et al.*, 2004*a*,*b*).

Following a standard procedure (Reed *et al.*, 1999), the electrolytic extraction of the $Cr_2N$ precipitates was carried out by immersing the aged specimen in an electrolyte consisting of 10% HCl + 1% tartaric acid ($C_4H_6O_6$) in methanol. A current density of 2 mA mm$^{-2}$ was used for 150 h, the density being measured on the sample, which was maintained as the anode. This technique has been shown to dissolve the $\gamma$ matrix only, although the extracted material can contain a small amount of $\gamma$ owing to the extremely small amount of $Cr_2N$. The electrolyte temperature was maintained between 273 and 303 K by adding cold water to a water bath as the extraction procedure was occurring. The extracted residue was washed carefully in methanol and collected on electrolyte-resistant filter paper using a water-jet pump system, in preparation for neutron powder diffraction.

The neutron diffraction experiments were carried out on HANARO (HANARO Center, Korea Atomic Energy Research Institute). Diffraction patterns were measured with a high-resolution powder diffractometer equipped with 32 detectors ($\Delta d/d \simeq 2.0 \times 10^{-3}$, where $d$ is the spacing of the diffraction peaks). The neutron beam was monochromated to a wavelength of 1.84 Å, and its spatial extension at the specimen level was 30 mm × 60 mm. The data were collected at intervals of 0.05° between 10 and 155° in the $2\theta$ range, with a sample rotation of *ca* 30 r.p.m. The program *FULLPROF* (Rodriguez-Carvajal, 1998) was used for the Rietveld refinement calculations [profile function: Gaussian + Lorentzian function (< 2%); important fitting parameters: lattice parameters, atom positions, occupancies of N atoms, background, peak width, peak anisotropy]. The nuclear scattering lengths used were $b$(Cr) = $0.3635 \times 10^{-12}$ cm and $b$(N) = $0.9360 \times 10^{-12}$ cm. In order to compare the ideal with the real crystal structure of $Cr_2N$, computer simulations of *SAD* patterns based on the measured crystallographic information for $Cr_2N$ were carried out using *Desktop Microscopist* V2.2 software (Lacuna Laboratories, USA). Thermodynamic calculations using the Thermo-Calc databank (Anderson *et al.*, 2002) with the TCFE2000 database were performed to obtain information on the phase equilibrium and the chemical composition of constituent phases.

## 3. Results

### 3.1. Brief description of the ordered $Cr_2N$ superstructure

The ordered $Cr_2N$ superstructure was characterized by three sets of superlattice reflections, namely (001), $(\frac{1}{3}\frac{1}{3}0)$ and $(\frac{1}{3}\frac{1}{3}1)$ [Fig. 4 of Lee *et al.* (2005)], and the crystallographic information on these reflections was summarized previously [Table 5 of Lee *et al.* (2006)]. A schematic illustration of the crystal structure of ordered $Cr_2N$ ($P\bar{3}1m$) based on an $\varepsilon$-type occupational-ordering model is shown in Fig. 1 (all the digits for lattice parameters, interatomic distances and N-atom occupancies were modified following the analyses of neutron diffraction in the present study). The unit cell based on the

**Table 1**
Comparison between ideal and measured $Cr_2N$ superstructures (the standard deviations for refining the neutron diffraction pattern are specified in parentheses).

Ordered $Cr_2N$ superstructure (trigonal, space group $P\bar{3}1m$).

| | | Atom position | | Occupancies | |
|---|---|---|---|---|---|
| Atom | Wyckoff position | Ideal | Refined | Ideal | Refined |
| Cr | 6(*k*) | $x = 0.333$<br>$y = 0.000$<br>$z = 0.250$ | $x = 0.346$ (8)<br>$y = 0.000$<br>$z = 0.244$ (6) | 1.0 | 1.0 |
| N | 1(*a*) | (000) | | 1.0 | 1.00 (5) |
| | 1(*b*) | $(00\frac{1}{2})$ | | 0.0 | 0.00 |
| | 2(*d*) | $(\frac{1}{3}\frac{2}{3}\frac{1}{2})$ and $(\frac{2}{3}\frac{1}{3}\frac{1}{2})$ | | 1.0 | 0.74 (9) |
| | 2(*c*) | $(\frac{1}{3}\frac{2}{3}0)$ and $(\frac{2}{3}\frac{1}{3}0)$ | | 0.0 | 0.12 (3) |

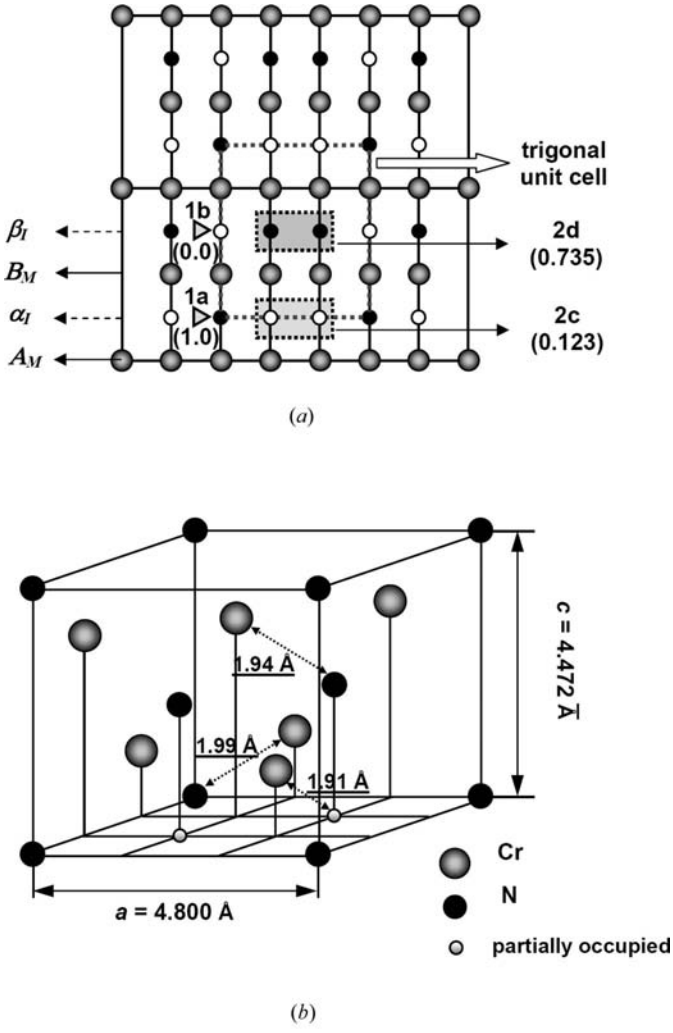


**Figure 1**
Schematic illustration of the ordered $Cr_2N$ superstructure based on an $\varepsilon$-type occupational ordering model; (*a*) the unit-cell based on the h.c.p. arrangement of Cr atoms and the six octahedral sites shown along the [210] projection (the measured N-atom occupancies in four Wyckoff sites are shown together), and (*b*) the resulting trigonal unit cell of $Cr_2N$ (the underlined digits represent the interatomic distances between metal and N atoms).

h.c.p. arrangement of Cr atoms consists of six Cr atoms and six interstitial sites for N atoms and vacancies. In the case of the ideal $Cr_2N$ superstructure, one N atom occupies the *A*1 site [Wyckoff position 1(*a*)] in the $\alpha_I$ plane, and the other two N atoms occupy *B*2 and *C*2 sites [Wyckoff position 2(*d*)] in the $\beta_I$ plane in the $Cr_2N$ superstructure owing to the repulsive interactions between them (Fig. 1*a*). The new crystal-coordinate system with the N atom at the origin corresponds to a trigonal structure with the space-group type $P\bar{3}1m$ (Fig. 1*b*). This $\varepsilon$-type occupational ordering of nitrogen leads to an increased $3^{1/2} \times 3^{1/2} \times 1$ superstructure.

### 3.2. N-atom distribution in the ordered $Cr_2N$ superstructure

Fig. 2 shows a typical neutron diffraction pattern and the corresponding Rietveld refinement of the electrolytically extracted specimen aged at 1173 K for $10^5$ s. Open circles are the measured intensities and the upper solid line represents the calculated fit. The line toward the bottom of the diagram represents an estimate of the difference between measured and calculated intensities, and the bars indicate the positions of the peaks that are identified. While the main diffraction peaks consist of the residual $\gamma$ matrix and the $Cr_2N$ precipitate, several extra peaks, which were not indexed in this study, also appeared with measurable intensities. These additional peaks presumably arise from a small amount of the intermetallic sigma ($\sigma$) phase, the existence of which was confirmed by TEM observations in our previous studies (Lee *et al.*, 2004*a*,*b*). However, it is not easy to refine the diffraction peaks from the $\sigma$ phase in that (i) the $\sigma$ phase contains a considerable number of diffraction peaks owing to its complex crystal structure [a tetragonal unit cell ($c/a = 0.52$, 30 atoms per unit cell) belonging to the space group $P4_2/mnm$ with lattice parameters $a = 8.80$ and $c = 4.54$ Å] and (ii) in our neutron diffraction experiment only a minor fraction of diffraction peaks were detected, which is not enough to refine and identify that phase. Therefore, the Rietveld refinement for the neutron diffraction pattern was restricted to two main phases, namely the $\gamma$ matrix and the $Cr_2N$ precipitate.

The lattice parameter of $\gamma$ was determined to be 3.627 (2) Å with space group $Fm\bar{3}m$, and there was no preferential texture, as expected. (For the lattice parameter, the three significant digits below the decimal point were used in this study after the Rietveld refinement.) It was possible to obtain reasonable agreement between the measured and calculated diffraction patterns with the aid of Rietveld refinement, and this enabled detailed crystallographic information on the ordered $Cr_2N$ superstructure to be estimated. The crystallographic information on the measured $Cr_2N$ superstructure and the ideal structure is summarized in Table 1, and the modified unit-cell dimensions together with the N-atom occupancies are illustrated in Fig. 1.

The crystal structure of ordered $Cr_2N$ was confirmed as trigonal, belonging to the space group $P\bar{3}1m$, and the lattice parameters were determined to be $a = 4.800$ (4) and $c = 4.472$ (5) Å, which are larger than those determined for pure binary $Cr_2N$ in previous studies (Kim *et al.*, 1990; Vallas &

**Table 2**
Chemical composition of $Cr_2N$ (measured and calculated, unit wt%).

| | Fe | Cr | Mn | Mo | C | N |
|---|---|---|---|---|---|---|
| Measured | Balance | 77.81 | 12.06 | 3.53 | – | – |
| Calculated | Balance | 55.55 | 19.39 | 4.12 | 0.111 | 9.104 |

Calvert, 1985). The volume of the unit cell was calculated to be 89.203 Å$^3$, and the chemical composition of the unit cell is $M_{5.546}X_{2.716}$, namely $M_2X_{0.979}$, indicating a slight deficiency of interstitial atoms within the $Cr_2N$ superstructure. According to the $\varepsilon$-type ordering model, the dimensions of an h.c.p. sublattice of metal atoms were calculated as $a$ = 2.771 and $c$ = 4.472 Å, which is slightly larger than those ($a$ = 2.748 and $c$ = 4.438 Å) reported in previous studies (Andrews *et al.*, 1971; The Bristol Group, 1984). This difference in lattice parameters is attributed to the dissimilar chemical composition of $Cr_2N$; while $Cr_2N$ in the previous studies was the pure binary compound, the $Cr_2N$ precipitate in the present study is actually an $M_2X$-type compound partially composed of several other alloying elements, *viz*. Fe, Mo and Mn as substitutional and C as interstitial constituents. Among the aforementioned substitutional elements, it is known that Mo, with a larger atomic radius [Cr: 1.20 Å; Mo: 1.40 Å in 12-coordinated metals (Pearson, 1972)], has a strong propensity to form precipitates, leading to an increase in lattice parameters of the precipitates (Peckner & Bernstein, 1987; Weiss & Stickler, 1972). As an example, a typical chemical composition of $Cr_2N$ analysed using X-ray energy-dispersive spectrometry (XEDS) in TEM (Fig. 3) is given in Table 2, and, for comparison, the chemical composition of $Cr_2N$ in the equilibrium state, calculated using thermodynamic methods (*CALPHAD*), is also shown. A detailed description of the thermodynamic calculation is given by Lee *et al.* (2004*b*). TEM–XEDS analyses were carried out for relatively large precipitates lying in a thin area in order to minimize the interaction volume of the electron beam due to specimen thickness, and quantitative analyses were performed only for substitutional elements because the quantitative data for light elements are less reliable (Williams & Carter, 1996). As clearly seen in Table 2, the $Cr_2N$ sample included a significant amount of other substitutional elements such as Fe, Mo and Mn. Therefore, in contrast to the results for the pure binary specimen reported elsewhere (Andrews *et al.*, 1971; Kim *et al.*, 1990; Vallas & Calvert, 1985), the diffraction effect from $Cr_2N$ in this study may show complex features, as will be discussed later.

An initial refinement for N-atom occupancies was carried out using the ideal $Cr_2N$ structure: (i) Cr in 6($k$): $x$ = 0.333, $z$ = 0.250, and (ii) N in 1($a$) and 2($d$), as given in Table 1. This refinement gave a poor agreement between observed and calculated patterns, especially in intensities. Therefore, the occupancy parameters of nitrogen were allowed to change, analogous to other neutron diffraction studies (Epicier *et al.*, 1988; Hashimoto *et al.*, 1974; Hirabayashi *et al.*, 1974; Lönnberg *et al.*, 1986). By allowing nitrogen occupation of the remaining octahedral sites, namely 1($b$) and 2($c$) in Fig. 1($a$), the agreement between the calculated and measured intensities was further improved. The normalized occupancies of N atoms in four Wyckoff sites [1($a$), 1($b$), 2($d$) and 2($c$)] were determined to be 1.00 (5), 0.0, 0.74 (9) and 0.12 (3), respectively. This means that a partial disordering of N atoms occurred along the $c$ axis [between the 2($d$) and 2($c$) Wyckoff sites], whereas the 1($a$) and 1($b$) sites remained perfectly ordered. Similar partial disordering of interstitial atoms along the $c$ axis has been reported in other $\varepsilon$-$M_2X$-type superstructures having an identical space group (Epicier *et al.*, 1988; Lönnberg *et al.*, 1986) and in other space groups such as $Mo_2C_{1-x}$ (Epicier *et al.*, 1988) and $ZrO_x$ (0.30 $\leq x \leq$ 0.41) (Hashimoto *et al.*, 1974;

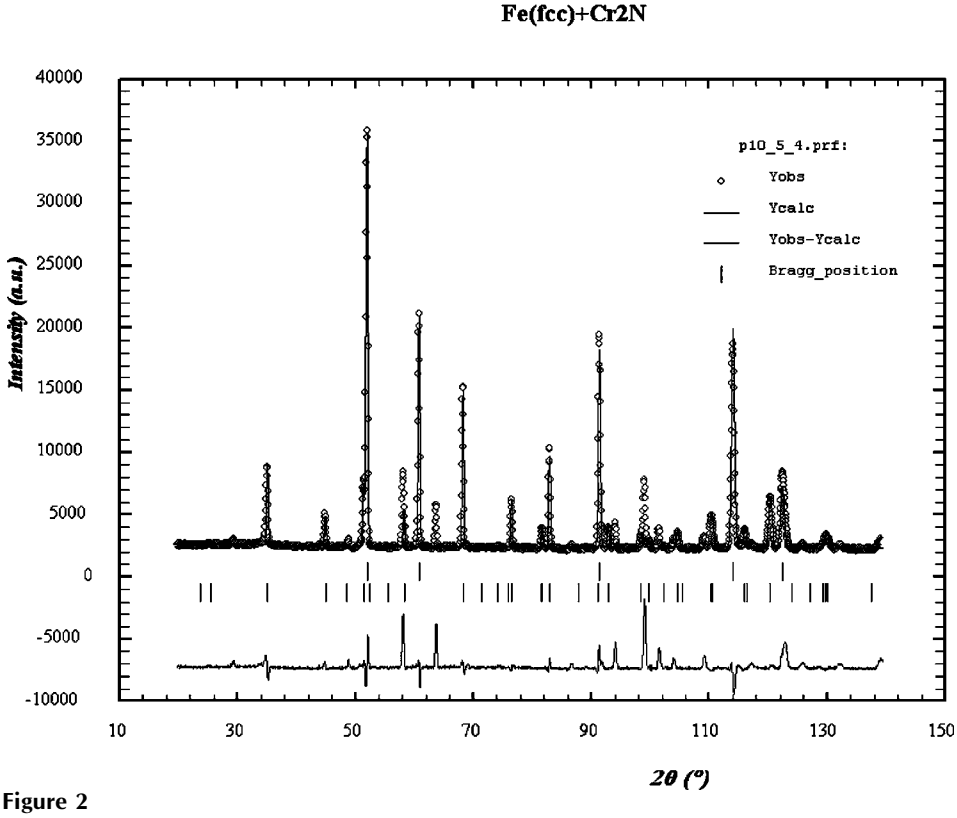


**Figure 2**
A typical neutron diffraction pattern and corresponding Rietveld refinement of an electrolytically extracted specimen aged at 1173 K for $10^5$ s. Circles are the observed intensities and the upper solid line represents the calculated fit. The lower solid line represents the difference. The two rows of small bars represent the Bragg reflection positions of austenite (upper) and $Cr_2N$ (lower).

**Table 3**
Relative intensities of superlattice reflections calculated on the basis of the ideal and measured configurations of the $Cr_2N$ superstructure.

| Superlattice reflections | Ideal | Measured |
|---|---|---|
| (001) | 12.7 | 19.5 |
| $(\frac{1}{3}\frac{1}{3}0)$ | 0.2 | 20.2 |
| $(\frac{1}{3}\frac{2}{3}0)$ | 0.3 | 2.8 |
| $(\frac{1}{3}\frac{1}{3}1)$ | 22.1 | 10.4 |
| $(\frac{1}{3}\frac{2}{3}1)$ | 15.0 | 7.6 |
| $(\frac{1}{3}\frac{1}{3}2)$ | – | 2.9 |
| $(\frac{1}{3}\frac{1}{3}4)$ | – | 6.1 |
| $(\frac{1}{3}\frac{2}{3}4)$ | – | 1.7 |

Hirabayashi *et al.*, 1974). According to these previous studies, it is worthwhile to note that the occupation of interstitial atoms in the 1(*b*) site was determined to be almost zero, irrespective of their composition and discrete crystal structures, which is in agreement with the present study.

### 3.3. Comparison between ideal and measured $Cr_2N$ superstructures

Apart from the partial disordering of the N atom along the *c* axis, another salient feature of the measured $Cr_2N$ superstructure is the deviation of metal atoms from their ideal positions. The position of the metal atom obtained from neutron diffraction is $x = 0.346\ (8)$, $y = 0$ and $z = 0.244\ (6)$, respectively. Compared with the ideal position ($x = 0.333$, $y = 0$ and $z = 0.250$), an expansion (3.9%) in the *x* direction and a contraction (−2.4%) in the *z* direction were detected. In order to manifest the different scattering effects induced by the deviation of metal atoms, a computer simulation of SAD patterns was carried out. The assumptions for the simulation of SAD patterns were as follows:

(i) the ideal and measured lattice parameters of $Cr_2N$ were set to be identical ($a = 4.800$ and $c = 4.472$ Å);

(ii) all the metal atoms were fixed to be Cr (the chemical composition of $Cr_2N$ can vary even in the same specimen; thus, it is impossible to determine the accurate fraction of other alloying elements);

(iii) in the relative intensities of the $Cr_2N$ structure, $(\bar{3}030)$ in the measured and (0002) in the ideal structure were set to be 100%, because they have the strongest calculated intensities.

Fig. 4 shows the SAD patterns of $Cr_2N$ obtained, and the computer simulations of SAD patterns based on both ideal and measured configurations of the $Cr_2N$ superstructure (Table 1). The relative intensities of superlattice reflections for characterizing the $Cr_2N$ superstructure are given in Table 3. Figs. 4(*a*) through 4(*c*) show the [001] SAD pattern with the highest symmetry and the computer-simulated SAD patterns of the $Cr_2N$ superstructure. The $(\frac{1}{3}\frac{1}{3}0)$-type reflection is the only superlattice reflection in this zone axis and corresponds to $(01\bar{1}0)$ and $(02\bar{2}0)$ in trigonal coordinates. The relative intensities of $(\frac{1}{3}\frac{1}{3}0)$ and $(\frac{1}{3}\frac{2}{3}0)$ in the measured $Cr_2N$ configuration were calculated to be 20.2 and 2.8, whereas those of ideal $Cr_2N$ were detectable but much lower (0.2 and 0.3). Comparing these with the real SAD pattern in Fig. 4(*a*), the observed intensities of $(\frac{1}{3}\frac{1}{3}0)$-type reflections had a closer resemblance to the calculated SAD pattern of the measured $Cr_2N$ configuration. Moreover, in our previous irradiation experiments with TEM, it was found that the $(\frac{1}{3}\frac{2}{3}0)$ superlattice reflection with lower scattering intensity compared with

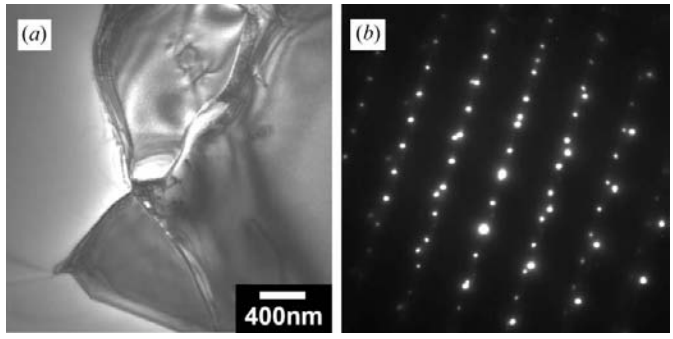


**Figure 3**
TEM micrographs of $Cr_2N$ precipitates: (*a*) BF (bright field) image and (*b*) SAD pattern ($z = [110]_\gamma // [01\bar{1}0]_{Cr_2N}$).

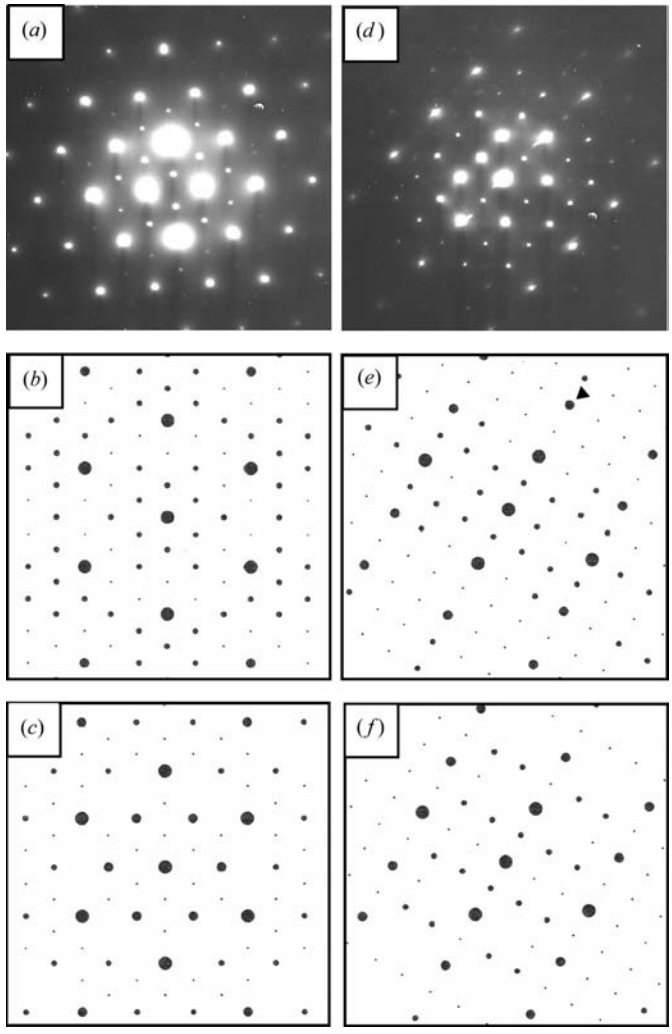


**Figure 4**
Comparison between the measured and ideal configurations of $Cr_2N$; (*a*) and (*d*) [001] and [100] SAD patterns of $Cr_2N$; (*b*) and (*e*) calculated SAD patterns of the measured $Cr_2N$ configuration; (*c*) and (*f*) calculated SAD patterns of the ideal $Cr_2N$ configuration.

($\frac{1}{3}\frac{1}{3}0$) disappeared in the first place, followed by extinction of the ($\frac{1}{3}\frac{1}{3}0$) superlattice reflection. Therefore, the calculated SAD pattern of Fig. 4(*b*) based on the measured atomic coordinate showed more reasonable agreement with experimental results.

As shown in our previous studies (Lee *et al.*, 2005, 2006), the most important SAD pattern showing all of the superlattice reflections for characterizing the $Cr_2N$ superstructure could be obtained in the [100] zone axis. In addition to the ($\frac{1}{3}\frac{1}{3}0$)-type superlattice reflection observed in the [001] zone axis, two other types of superlattice reflection can be distinguished in this zone axis. In the case of the measured configuration of $Cr_2N$ in Fig. 4(*e*), the relative intensities of the (001), ($\frac{1}{3}\frac{1}{3}1$) and ($\frac{1}{3}\frac{2}{3}1$) reflections were calculated to be 19.5, 10.4 and 7.6, respectively; those of ideal $Cr_2N$ in Fig. 4(*f*) are 12.7, 22.1 and 15.0, respectively. Although the calculated intensities of the two configurations showed small differences, the overall distribution looks almost the same irrespective of the detailed configuration of the $Cr_2N$ superstructure, meaning that the diffraction effects of these reflections are not affected by the configuration of the metal-atom position and partial disordering of N atoms. Because the (001)-type superlattice reflection reflects the modulation between the $\alpha_I$ and $\beta_I$ layers of interstitial atoms and the ($\frac{1}{3}\frac{1}{3}1$)-type superlattice reflection characterizes all the $\varepsilon$-type ordered structures (Epicier *et al.*, 1988; Hiraga & Hirabayashi, 1980; Lee *et al.*, 2005; Leineweber & Jacobs, 2000), these two types of superlattice reflections should occur, as shown in Table 1. Conversely, a more pronounced difference between the measured and ideal $Cr_2N$ superstructures lies in the intensities of high-order superlattice reflections such as ($\frac{1}{3}\frac{1}{3}2$), ($\frac{1}{3}\frac{1}{3}4$) and ($\frac{1}{3}\frac{2}{3}4$). As shown in Fig. 4(*f*), the ($\frac{1}{3}\frac{1}{3}2$), ($\frac{1}{3}\frac{1}{3}4$) and ($\frac{1}{3}\frac{2}{3}4$) reflections have no scattering intensities, although these reflections are clearly visible in the real SAD pattern in Fig. 4(*d*). On the other hand, the calculated SAD pattern based on the measured $Cr_2N$ superstructure has scattering intensities of 2.9, 6.1 and 1.7, respectively.

On the basis of the results of computer simulations of SAD patterns, it can be deduced that (i) the simulated results based on the measured $Cr_2N$ configuration are more realistic and show a reasonable intensity distribution and (ii) the deviation of metal atoms from their ideal positions has a profound effect on the scattering intensities of ($\frac{1}{3}\frac{1}{3}0$)-type superlattice reflections, whereas the other two types of superlattice reflection were not significantly affected by the deviation of metal atoms.

## 4. Discussion

### 4.1. On the ordered $Cr_2N$ superstructure

There are two salient features distinguishing the measured $Cr_2N$ superstructure from the ideal crystal structure:

(i) the deviation of metal atoms: metal atoms deviate from their ideal positions, and the intensities of the ($\frac{1}{3}\frac{1}{3}0$)-type superlattice reflections depend on the positions of the metal atoms;

(ii) the distribution of N atoms: as opposed to the ideal configuration of nitrogen, a partial disordering of N atoms occurs along the *c* axis, whereas the distribution of N atoms over the other 1(*a*) and 1(*b*) sites remains perfectly ordered.

The aforementioned discrepancies between the ideal and measured $Cr_2N$ superstructures can affect the diffraction intensities as well as the redistribution of N atoms during order–disorder transitions. The former is sensitive to both (i) and (ii); the latter is uniquely dependent on (ii). According to Fig. 4, quantitative statements on the comparison between the measured and ideal structures of $Cr_2N$ can be made in terms of three sets of superlattice reflections:

(i) (001)-type superlattice reflection: The relative intensities of the (001) reflection in the two structures were calculated to be 19.5 (measured) and 12.7 (ideal), which means that this reflection was not affected by the position of the metal atom and partial disordering of the N atoms. The (001) superlattice reflection is known to characterize the $\varepsilon$-$M_2X$-type superstructures and represents the modulation of the interstitial contents between the $\alpha_I$ and $\beta_I$ layers [$n(A1) + n(B1) + n(C1) \neq n(A2) + n(B2) + n(C2)$] in Fig. 1(*a*) (Epicier *et al.*, 1988; Hiraga & Hirabayashi, 1980; Lee *et al.*, 2005; Leineweber & Jacobs, 2000). Comparing the measured and ideal configurations of $Cr_2N$, this reflection can appear in both configurations, because the differences in nitrogen content between the $\alpha_I$ and $\beta_I$ layers are 0.22 (measured) and 1.0 (ideal). If further partial disordering between 2(*d*) and 2(*c*) occurs, leading to equilibration of the interstitial contents between these layers, then the (001) reflection may not be observed. Epicier *et al.* (1988) reported that the C-atom occupancies in $\varepsilon$-$W_2C$ are $n(A1) = 0.97$, $n(A2) = 0.03$, $n(B1 = C1) = 0.26$ and $n(B2 = C2) = 0.74$, *i.e.* the carbon contents in layers 1 and 2 are 1.49 and 1.51, respectively, and the (001) reflection could not be observed because the difference of carbon content in these two layers was negligibly small. On account of the lack of the (001) reflection, these authors proposed the intermediate $\varepsilon'$ structures, in which the ordering was incomplete with respect to a partial transfer of C atoms from 2(*d*) to 2(*c*) sites. Thus, the occurrence of the (001) superlattice reflection is strongly dependent on the degree of disordering of interstitial atoms along the *c* axis.

(ii) ($\frac{1}{3}\frac{1}{3}0$)-type superlattice reflection: The relative intensities of ($\frac{1}{3}\frac{1}{3}0$) and ($\frac{1}{3}\frac{2}{3}0$) in the measured $Cr_2N$ superstructure were calculated to be 20.2 and 2.8, whereas those of ideal $Cr_2N$ were as low as 0.2 and 0.3. The ($\frac{1}{3}\frac{1}{3}0$) superlattice reflection is known to characterize the $\varepsilon$-$M_3X$-type superstructure and reflects the modulation of the interstitial content between different channels *A*, *B* and *C* [$n(A1) + n(A2)$, $n(B1) + n(B2)$ and $n(C1) + n(C2)$ become unequal (Leineweber & Jacobs, 2000)]. In the case of ideal $Cr_2N$, this reflection did not appear because of the equal nitrogen content in channels *A*, *B* and *C*, as shown in Fig. 1(*a*). On the other hand, it is known that this reflection can also appear following the displacement of metal atoms from their ideal positions ($x = 0.333$, $y = 0$ and $z = 0.250$) (Hiraga & Hirabayashi, 1980; Leineweber & Jacobs, 2000) and is especially sensitive to the deviation of the *x* coordinate. Comparing the real SAD pattern in Fig. 4(*a*), it is obvious that

the real intensities of $(\frac{1}{3}\frac{1}{3}0)$ and $(\frac{1}{3}\frac{2}{3}0)$ are in good agreement with the measured $Cr_2N$ superstructure rather than the ideal configuration of the $x$ coordinate. Therefore, it can be deduced that the metal atoms deviate from their ideal positions, which causes the $(\frac{1}{3}\frac{1}{3}0)$-type superlattice reflection to appear clearly. In addition, it was found that the $(\frac{1}{3}\frac{2}{3}0)$ reflection disappeared prior to $(\frac{1}{3}\frac{1}{3}0)$ during the order–disorder transition. The prior disappearance of the $(\frac{1}{3}\frac{2}{3}0)$ reflection probably results from the relatively low intensity compared with the $(\frac{1}{3}\frac{1}{3}0)$ reflection.

(iii) $(\frac{1}{3}\frac{1}{3}1)$-type superlattice reflection: This reflection is known to characterize all the $\varepsilon$-type ordered structures irrespective of their interstitial content (Lee *et al.*, 2005; Leineweber & Jacobs, 2000). The relative intensities of the $(\frac{1}{3}\frac{1}{3}1)$ and $(\frac{1}{3}\frac{2}{3}1)$ reflections are 10.4 and 7.6 in the measured and 22.1 and 12.7 in the ideal structure of $Cr_2N$, respectively. As expected, these superlattice reflections have reasonable intensities irrespective of metal-atom deviation and partial disordering of nitrogen.

(iv) High-order superlattice reflections: One of the pronounced differences between the measured and ideal $Cr_2N$ superstructures is in the intensities of high-order superlattice reflections such as $(\frac{1}{3}\frac{1}{3}2)$, $(\frac{1}{3}\frac{1}{3}4)$ and $(\frac{1}{3}\frac{2}{3}4)$. As shown in Fig. 4(*f*), the $(\frac{1}{3}\frac{1}{3}2)$, $(\frac{1}{3}\frac{1}{3}4)$ and $(\frac{1}{3}\frac{2}{3}4)$ reflections have no scattering intensities, although these reflections are clearly visible in the real SAD pattern in Fig. 4(*d*). On the other hand, the calculated SAD pattern based on the measured $Cr_2N$ superstructure has reasonable scattering intensities.

### 4.2. On the order–disorder transition of $Cr_2N$

In our previous study (Lee *et al.*, 2006), the superlattice reflections were found to disappear sequentially, (001) $\rightarrow$ $(\frac{1}{3}\frac{1}{3}0) \rightarrow (\frac{1}{3}\frac{1}{3}1)$, during electron irradiation within TEM. On the basis of this observation, an order–disorder model for $Cr_2N$ can be expounded in a two-step process, *i.e.* the redistribution of N atoms sequentially occurs (i) along the $c$ axis and then (ii) perpendicular to the $c$ axis until the nitrogen configuration attained is that of the disordered structure. Given that the configuration of N atoms in the 2(*d*) and 2(*c*) Wyckoff sites is unstable compared with other sites, it may be easier for nitrogen to move and redistribute between these sites during the order–disorder transition. Moreover, the interatomic distance between 2(*d*) and 2(*c*) is calculated to be 2.24 Å, which is shorter than that between 2(*d*) and 1(*b*) or 2(*c*) and 1(*a*) (2.77 Å). Therefore, it can be deduced that the partial disordering of nitrogen along the $c$ axis detected in neutron diffraction analysis supports an order–disorder model for $Cr_2N$ suggested by the present authors.

Lönnberg *et al.* (1986) suggested that the interatomic distance between the 1(*b*) site and the six nearest neighboring W atoms is shorter than the shortest C—W distance, which makes it difficult for C atoms to accommodate the 1(*b*) hole. In contrast to the results for the W–C system, the interatomic distance between the N atom in the 1(*b*) site and the nearest neighboring Cr atoms was measured to be 2.02 Å in the present case, which is larger than the Cr—N distances in other octahedral sites, as shown in Fig. 1. Thus, the explanation based on interatomic distances is not applicable to the Cr–N system. On the other hand, in the case of the Cr–N system, it is reported that the N–Cr ($-144.03$ kJ mol$^{-1}$) and Cr–Cr ($-56.10$ kJ mol$^{-1}$) interactions are both attractive and the former is more attractive than the latter, whereas the interaction of between N atoms (33.49–95.88 kJ mol$^{-1}$ depending on temperature) is repulsive (Shohoji *et al.*, 1974). On account of the strong repulsive interaction between N atoms, the preferential vacancy in the 1(*b*) site can be explained as follows: the nitrogen content in the $\beta_I$ plane is twice that in the $\alpha_I$ plane; if the repulsive interaction between N atoms is so strong that partial transfer of N atoms along the $c$ axis tends to occur, it is more probable for N atoms to move from 2(*d*) to 2(*c*) rather than from 1(*a*) to 1(*b*) owing to the larger population in the $\beta_I$ plane.

Epicier & Esnouf (1984) carried out irradiation of ordered $\varepsilon$-$W_2C$ within an electron microscope. They reported that the C atoms are more easily displaced when the electron beam is perpendicular to the $c$ axis rather than parallel, indicating that carbon diffusion across the basal planes of the metal atoms is more difficult. Later, Leineweber *et al.* (2001) studied the magnetic structure and disorder of nitrogen in $\varepsilon$-$Fe_3N$ and suggested that the disordering occurred through the nitrogen redistribution perpendicular to the $c$ axis from the 2(*c*) to the 2(*b*) Wyckoff position above 450 K. They also explained that nitrogen redistribution along the $c$ axis is difficult because the occupancy for the 2(*d*) Wyckoff position was not changed during the order–disorder transition. Contrary to these previous studies, in the case of $Cr_2N$, the order–disorder transition was initiated through the partial transfer of N atoms along the $c$ axis rather than perpendicular to the $c$ axis; this explanation is supported by the disappearance of the (001) superlattice reflection. However, it is worthwhile to note that the order–disorder transition could have phenomenological differences depending on the alloy systems and interstitial distribution, because the movement of interstitial atoms shows a dissimilar trend following the atomic interactions as well as the degree of disordering of interstitial atoms within octahedral or tetrahedral sites in these ordered structures.

## 5. Conclusions

The neutron diffraction study on the ordered $Cr_2N$ superstructure in high-nitrogen austenitic Fe–18Cr–18Mn–2Mo–0.9N steel is summarized as follows.

On the basis of the Rietveld refinement of neutron diffraction patterns, the ordered $Cr_2N$ superstructure was confirmed to be ordered h.c.p. or trigonal (space group $P\bar{3}1m$) with lattice parameters $a$ = 4.800 (4) and $c$ = 4.472 (5) Å.

The occupancies of the N atoms in four crystallographic sites [1(*a*), 1(*b*), 2(*d*) and 2(*c*) Wyckoff sites] were determined to be 1.00 (5), 0.0, 0.74 (9) and 0.12 (3), respectively. This means that a partial disordering of N atoms occurred along the $c$ axis, which can support the order–disorder model suggested by the present authors.

The position of the metal atom was found to be $x$ = 0.346 (8) and $z$ = 0.244 (6), corresponding to a deviation from the ideal

position ($x$ = 0.333 and $z$ = 0.25). This deviation has a drastic effect on the scattering intensities of the $(\frac{1}{3}\frac{1}{3}0)$-type superlattice reflection, whereas the other two types of superlattice reflection are not significantly affected by a deviation of the metal atoms.

On the basis of the results of computer simulation of SAD patterns, the result for the measured $Cr_2N$ configuration was more realistic and showed a reasonable intensity distribution.

This work was financially supported by the Ministry of Commerce, Industry and Energy of Korea. One of the authors (Tae-Ho Lee) acknowledges the financial support provided by the Japan Society for the Promotion of Science through the dissertation PhD program. The authors also express their gratitude to Hae-Jung Bang and Sung-Tae Kim of Pusan National University for valuable help in experimental work of electrolytic extraction.

## References

Anderson, J. O., Helander, T., Höglund, L., Shi, P. & Sundman, B. (2002). *CALPHAD*, **26**, 273–312.
Andrews, K. W., Dyson, D. J. & Keown, S. R. (1971). *Interpretation of Electron Diffraction Patterns*, p. 203. London: Hilger.
Ducastelle, F. (1991). *Order and Phase Stability in Alloys*, p. 162. North Holland: Elsevier Science Publishers BV.
Epicier, T., Dubois, J., Esnouf, C., Fantozzi, G. & Convert, P. (1988). *Acta Metall.* **36**, 1903–1921.
Epicier, T. & Esnouf, C. (1984). *J. Microsc. Spectrosc. Electron.* **9**, 17–28.
Gavriljuk, V. G. & Berns, H. (1999). *High Nitrogen Steels*, p. 135. Berlin: Springer-Verlag.
Hashimoto, S., Iwasaki, H., Ogawa, S., Yamaguchi, S. & Hirabayashi, M. (1974). *J. Appl. Cryst.* **7**, 67–73.
Hendricks, S. B. & Kosting, P. B. (1930). *Z. Kristallogr.* **74**, 511–533.
Hirabayashi, M., Yamaguchi, S., Arai, T., Asano, H. & Hashimoto, S. (1974). *Phys. Status Solidi*, **23**, 331–339.
Hiraga, K. & Hirabayashi, M. (1980). *J. Appl. Cryst.* **13**, 17–23.
Jack, K. H. (1952). *Acta Cryst.* **5**, 404–411.
Khachaturyan, A. G. (1978). *J. Prog. Mater. Sci.* **22**, 1–150.
Khachaturyan, A. G. (1983). *Theory of Structural Transformations in Solids*, pp. 39–95. New York: John Wiley.
Kikuchi, M., Kajihara, M. & Choi, S. K. (1991). *Mater. Sci. Eng. A*, **146**, 131–150.
Kim, S. J., Marquart, T. & Franzen, H. F. (1990). *J. Less-Common Met.* **158**, L9–L10.
Landau, L. D. & Lifshitz, E. M. (1980). *Statistical Physics Part I*, pp. 401–516. Oxford: Pergamon Press.
Lee, T. H., Kim, S. J. & Jung, Y. S. (2000). *Metall. Mater. Trans. A*, **31**, 1713–1723.
Lee, T. H., Kim, S. J. & Takaki, S. (2006). *Acta Cryst.* B**62**, 190–196.
Lee, T. H., Oh, C. S., Han, H. N., Lee, C. G., Kim, S. J. & Takaki, S. (2005). *Acta Cryst.* B**61**, 137–144.
Lee, T. H., Oh, C. S., Lee, C. G., Kim, S. J. & Takaki, S. (2004*a*). *Met. Mater. Interact.* **10**, 231–236.
Lee, T. H., Oh, C. S., Lee, C. G., Kim, S. J. & Takaki, S. (2004*b*). *Scr. Mater.* **50**, 1325–1328.
Leineweber, A. & Jacobs, H. (2000). *J. Alloys Compd.* **308**, 178–188.
Leineweber, A., Jacobs, H., Hüning, F., Lueken, H. & Kockelmann, W. (2001). *J. Alloys Compd*, **316**, 21–38.
Lönnberg, B., Lundström, T. & Tellgren, R. (1986). *J. Less-Common Met.* **120**, 239–245.
Nagakura, S. & Oketani, S. (1968). *Trans. ISIJ*, **8**, 265–294.
Pearson, W. B. (1972). *Crystal Chemistry and Physics of Metals and Alloys.* New York: Wiley-Interscience.
Peckner, D. & Bernstein, I. M. (1987). *Handbook of Stainless Steel*, pp. 4–35. New York: McGraw Hill Inc.
Reed, R. C., Jackson, M. P. & Na, Y. S. (1999). *Metall. Mater. Trans. A*, **30**, 521–533.
Rodriguez-Carvajal, J. (1998). *FULLPROF*, Version 3.5d. Laboratoire Leon Brillouin, Saclay, France.
Shohoji, N., Katsura, M. & Sano, T. (1974). *J. Less-Common Met.* **38**, 59–70.
Simmons, J. W. (1996). *Mater. Sci. Eng. A*, **207**, 159–169.
The Bristol Group (1984). *Convergent Beam Electron Diffraction of Alloy Phases*, p. 61. Bristol/Boston: Adam Hilger.
Vallas, P. & Calvert, L. D. (1985). *Pearson's Handbook of Crystallographic Data for Intermediate Phases*, Vol. 2, p. 1877. Materials Park, OH, USA: ASM.
Vanderschaeve, F., Taillard, R. & Foct, J. (1995). *J. Mater. Sci.* **30**, 6035–6045.
Weiss, B. & Stickler, R. (1972). *Metall. Trans. A*, **3**, 851–856.
Williams, D. B. & Carter, C. B. (1996). *Transmission Electron Microscopy – A Textbook for Materials Science*, p. 553. New York/London: Plenum Press.